

An Integrated Study of Gravity and Magnetic Data on West El-Minya Area, Western Desert, Egypt.Saada¹ S. A. and El-Khadragy² A. A.¹-Faculty of Science, Geology Department, Suez University, Suez, Egypt.² Faculty of Science, Geology Department, Zagazig University, Zagazig, Egypt.saada_geo@yahoo.com

Abstract: The potential field data in the West El-Minya area had been analyzed to delineate the regional subsurface structural and tectonic framework of the buried basement rocks. To achieve this goal, several techniques are applied on both gravity and magnetic data. Trend analysis is applied on gravity and magnetic maps to define the major subsurface tectonic trends. Regional-residual separation was carried out using two methods (filtering analysis technique and least-squares polynomial fitting). In addition, depths to the basement rocks were estimated by using spectral analysis technique along 28 profiles. Moreover, Bouguer gravity and RTP anomalies are used with the drilled wells to construct gravity and magnetic models of the earth's crust along four profiles trending in N-S, NE-SW and E-W directions. These models divided the upper crust into two portions, the first upper one is composed of several blocks with different densities and magnetic susceptibilities while, the lower one has no magnetic susceptibilities. They show also the depths of the Conrad discontinuity vary from 21.2 to 24.7km and Moho discontinuity ranges from 30.5 to 34.9km. The computed depths were used to construct the basement relief map which shows that the depth to the basement rocks ranges from 0.5 to 4.2km. The results of quantitative techniques were integrated together to construct structure map of the study area. This map is mainly composed of faulted basement rocks of alternated uplifted and down-lifted blocks in NE-SW intersected by younger NNW- SSW transform faults.

[Saada S. A. and El-Khadragy A. A. **An Integrated Study of Gravity and Magnetic Data on West El-Minya Area, Western Desert, Egypt.** *J Am Sci* 2015;11(12):169-184]. (ISSN: 1545-1003). <http://www.jofamericanscience.org>. 23. doi:[10.7537/marsjas111215.23](https://doi.org/10.7537/marsjas111215.23).

Keywords: El-Minya- FFT- 2D crustal modeling- structure map.

1. Introduction

The study region lies to the west of El-Minya City as a part of the Egyptian Western Desert. It locates between latitudes 27° 30' - 29° 00' N and longitudes 29° 30' - 30° 30' E (Fig. 1). This study investigates the nature and the structure of the earth's crust as well as to construct the basement structure and basement relief maps.

The data include the Bouguer gravity and the Reduced to Pole (RTP) aeromagnetic maps, aided by the available surface and subsurface geological and geophysical information carried out on the investigated surrounding areas.

These data are analyzed and interpreted qualitatively and quantitatively through the following steps, (i) description of the gravity and magnetic maps; (ii) trend analysis technique; (iii) isolation of gravity and magnetic anomalies into their deep (regional) and near-surface (residual) components using the Fast Fourier Transform and the least squares polynomial technique; (iv) determination of depth to basement surface using 28 selected gravity and magnetic profiles distributed all over the area using spectral analysis technique; (v) constructing 2.5-D and 2-D magnetic-gravity modeling along four profiles, (vi) deducing the basement relief map and finally; (vii) construction of structure basement map.

The previous works that were carried out on the Western Desert by different authors are of regional studies. In this paper, we applied different analytical techniques to deduce a detailed structural basement map and to study the crustal thickness variations of the selected area using coupled gravity and magnetic modeling.

2. General Geology and Tectonics

The region was subjected to many cycles of sea regressions and transgressions with different tectonic activities, which are responsible for giving the area its recent stratigraphical and structural pattern.

The outcrops of this area (Fig 1) are composed of rocks and sediments belonging to the Eocene, Oligocene, Miocene and Quaternary ages. Eocene deposits (T_e) are composed mainly from the thick marine limestone with chert and minor clay beds. Oligocene deposits (T_o) are represented by fluvial and lacustrine clastics and gravel sheets. While, Miocene deposits are not observed in the area (they outcrop only north latitude 29° in Western Desert) except for very small basalt -dolerite dykes and sheets (T_v). Undivided Quaternary deposits (Q), mainly alluvial deposits of sand and gravel, are outcropped in the middle part. Moreover, sand dunes (Q_d) running generally in a NNW direction represent the Pliocene-Recent are present, especially in the eastern and

southwestern (Ghard Abu Muharik) parts of the investigated area. Sabkha deposits (Q_{sb}) are present in

the northeastern corner.

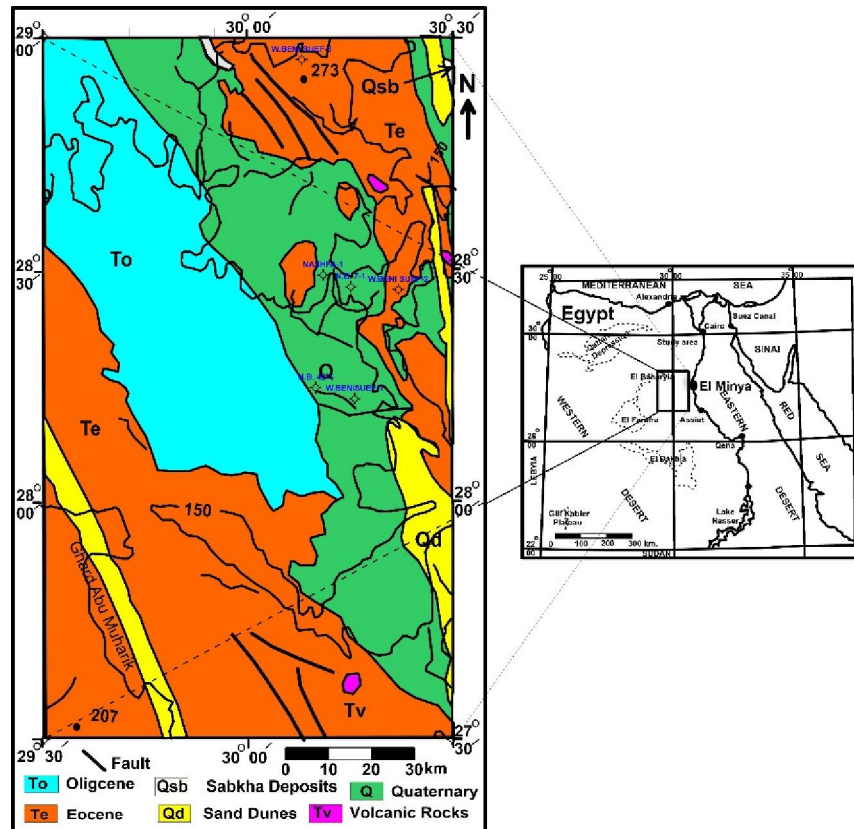


Fig 1. Location map shows the names and the locations of drilled wells as well as the geologic map of the study area (after Egyptian Geological Survey and Mining Authority 1981).

Structurally, it is well known that, the northern Western Desert, where the study area is included, lies on the margin of the unstable mobile belt of the tectonic framework of the Egyptian Territory (Said 1962). Consequently, a shallow and rugged basement rocks characterize it. The sedimentary succession of highly printed complex structural effects is represented by asymmetric linear folding, and faulting. The investigated area has been subjected to different tectonic regimes since Pre-Cambrian time to Recent. Pre-Cambrian exhibit three tectonic trends namely, Nubian (N-S), Red sea (NNW) and Tibesti (NE) trends, which are inherited in basement rocks of the northern Western Desert (Meshref 1990 and 1995). New tectonic trend appeared during Paleozoic time resulted from thrusting or uplifting of Africa continent against the main block of the earth's crust might have been cause of the formation of E-W trend. This trend is shown in the Gulf of Suez and northern Western Desert in Regional magnetic and isopach maps (Meshref 1990). In addition, strong E-W tectonic trend is shown in many parts of isopach maps of successive formation (e.g. Masajid and Khattatba

formation) of Middle-Upper Jurassic, which indicating that the deposition of sediments from Late Paleozoic to Late Jurassic was controlled by E-W tectonic trends (Meshref 1990).

Younger events appear in Late Jurassic to Early Tertiary resulted from movements of Africa relative to Eurasia (Tethyan plate movement). These activity appear in two phases (Hantar 1990, Meshref 1990 and Sultan & Abdel Halim 1988); (1) The Sinistral shear movements during Late Jurassic to Early Cretaceous (Nevadian event), so two tectonic elements recorded with wrench master E-W faults, NW fold which associated thrust faults and ENE strike slip faults (Dolson et al. 2001). (2) The Dextral shear movements that took place during Late Cretaceous to Early Tertiary (Laramide event). Therefore, two tectonic elements recorded with wrench master E-W faults, ENE fold (Syrian arc system) trend which associated thrust faults and WNW strike slip faults. After dextral lateral movements in Late Cretaceous to Early Tertiary followed by northward motion of Africa toward Eurasia produced the Alpine orogeny, where two compressive forces N-S and NNW-SSE trend

resulted (Youssef 1968 and Dietz & Hoden 1970). Many researchers (e.g. Said 1962; Abu El Ata 1981 and 1988; Meshref 1982, 1990, 2002; Dennis 1984; Abdel Aal and Moustafa 1988; Sultan and Abdel Halim 1988; El-Kenawy 2000 and others) dealt and are still dealing with these surface and subsurface structures.

Stratigraphically, the investigated area exhibits rocks ranging in age from Cambrian to Recent, as shown from the five drilled wells reached basement rocks (N. B. 42-1, Nashfa-1, W. Beni Suef-1, 2, and 3) (Fig 1). Barakat 1984 subdivided the completely sedimentary section of the northern Western Desert into the lower clastic (Cambrian to Early Mesozoic), the middle calcareous (Cenomanian to Late Eocene), and the upper clastic (Oligocene to Recent) divisions.

3. Data Processing, Interpretation and Results

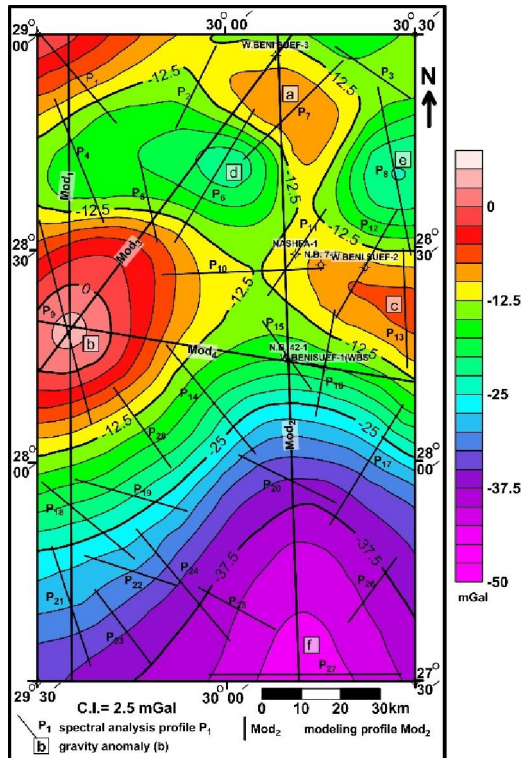


Fig 2. Bouguer map of the study area (after GPC 1984, the contour interval is of 2.5 mGal, showing the location of depth estimation profiles (P_1 to P_{28}) and crustal modeling profiles (Mod_1 to Mod_4))

The gravity data measured by General Petroleum Company (GPC) in 1984 (scale 1:250,000 and the contour interval is of 2.5mGal) are shown in Figure 2. The reduced to pole (RTP) magnetic data, measured by General Petroleum Company (GPC) in 1989 (scale 1:250,000 and the contour interval is of 25 nT) are shown in Figure 3. The interpretation of these maps

will be very useful for determining the relief and depths of the basement surface in the area.

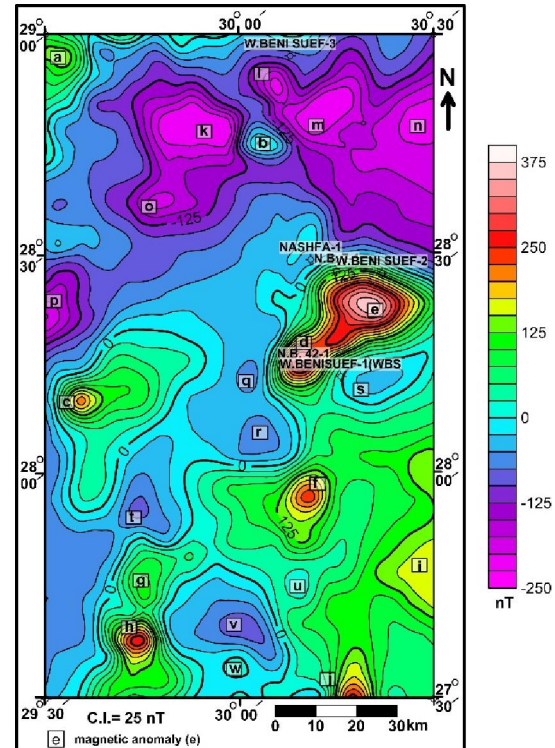


Fig 3 RTP magnetic map (GPC 1989), the contour interval is of 25 nT

3.1- Qualitative interpretation

Qualitative interpretation is considered as an attempt to get a rapid and rough overview of the observed potential fields and their relation to the geological situation of the investigated area through description of the recorded potential field.

3.1.1 Bouguer anomaly map

The Bouguer gravity anomaly map (Fig 2) reveals three positive (a, b and c) and negative (d, e and f) gravity anomalies with different sizes, shapes, trends, and extensions exhibiting nearly steady or gentle gradients all over the study area. A positive gravity belt (Fig 2, b and c), trending ENE to E-W direction, locates in the central part of the study area between latitudes $28^{\circ} 00'$ - $28^{\circ} 30'$ N. This belt consists of two anomalies with amplitudes range between -13 and 5 mGal. In addition, another positive anomaly (Fig 2, a) lies in the northern part. Moreover, a large zone characterized by negative gravity anomalies is located in the southern part of the study area with minimum amplitude of about -45 mGal (Fig 2, f). Other two negative gravity anomalies (Fig 2, d and e) are shown in the northern area trending in the WNW to E-W and NE directions with values ranging from -23 to -12.5 mGal. The negative anomalies may be

attribute to thick sedimentary cover. While, the positive ones may reflect the basement relief irregularities as well as the variations in the thickness and density heterogeneities in the crustal layer respectively because of the relatively regional nature of the contours extend.

3.1.2 RTP magnetic map:

The RTP magnetic map (Fig 3) reveals a series of positive (a, b, c,...j) and negative (k, l, m,w) magnetic anomalies with different sizes, shapes, trends, and extensions with nearly sharp and gentle gradients all over the study area. A maximum positive magnetic belt (includes c, d and e anomalies), trending ENE direction, is located at the central part of the study area with amplitudes ranging from 0- 370 nT. The southeastern part is characterized by the presence of positive anomalies (Fig 3, f to j) with amplitudes reaching 250 nT and displaying N-S to NE trends. Moreover, a large low magnetic zone (includes c, d and e anomalies) extends in the NE direction all over the area alternated with the previously positive ones with minimum amplitude of about -200nT in the northern part. Generally, the area contains many closed positive and negative anomalies orienting in N-S, NW and ENE directions with different amplitudes indicating three-dimensional bodies mainly related to the basement complex. Linear anomalies are also represented in the area with zones of maximum gradient that generally are associated with faults.

3.2 Quantitative interpretation

3.2.1 Analysis of tectonic trends

The trend analysis is a method by which the tectonic setting of the area is determined, where the tectonic history of rocks is, in some degree, recorded from the magnitude and the pattern of the gravity and

the magnetic anomalies (Affleck 1963). Both Bouguer anomaly and RTP magnetic maps (Figs 2 and 3) indicate that, the area is characterized by a complex pattern of major and minor faults. In order to study this tectonic history using Affleck's (1963) technique, the trends of both gravity and magnetic maps are determined. These determined trends are counted (N) and measured (both Lengths (L), in the unit of the map scale (km), and Azimuth, in degrees from the North). According to their directions around the north (clockwise and anticlockwise), they are distributed in a 10° spectrum (Tables 1 and 2). Then, they were statistically studied to calculate their numbers and lengths percentages (N% and L%). Their diagram (Fig 4) is also constructed to illustrate the Azimuth-Length percentages distributions of them.

Trend analysis of the Bouguer anomaly map shows that, N-S (N5°W-N5°E, Nubian or East-African), NE (N35°-45°E, Tibesti, Aualitic or Bukle), E-W (N85°E-N85°W, Tethyan or Mediterranean) trends are the main trends of the study area. The WNW (N55°-65°W, Najd, or Darag), ENE (N55°-75° E, Syrian Arc, Qattara, or North Sinai folds), and NW (N25°-45°W, Suez, Red Sea or Clysmic) trends are also represented in the study area with a decreasing order (Moody 1961; Said 1962; Abdel Gawad 1970; El-Shazly et al. 1975; Halsey and Gardner 1975). While, the trends deduced from RTP magnetic map show clearly that, WNW, NW, N-S, ENE, E-W (Tethyan or Mediterranean), NE, and NNE (N15°-25° or Aqaba) trends are affecting the basement rocks of the study. This difference in the arrangements indicate that, N-S E-W trends are rejuvenated so, they intersected the sedimentary rocks and recorded in the Bouguer gravity map.

Table 1 Parameters (numbers (N), lengths (L), number and lengths percentages (N% and L%) of the major fault trends detected from Bouguer anomaly map.

WEST				Azimuth	EAST				
N	N%	L(km)	L%		L%	L(km)	N%	N	
2.0	18.2	116.7	28.7	0:<10	0.0	0.0	0.0	0.0	
0.0	0.0	0.0	0.0	10:<20	0.0	0.0	0.0	0.0	
1.0	9.1	26.7	6.5	20:<30	0.0	0.0	0.0	0.0	
0.0	0.0	0.0	0.0	30:<40	17.4	70.7	18.2	2.0	
0.0	0.0	0.0	0.0	40:<50	5.9	23.9	9.1	1.0	
2.0	18.2	70.5	17.3	50:<60	6.6	27.0	9.1	1.0	
0.0	0.0	0.0	0.0	60:<70	0.0	0.0	0.0	0.0	
0.0	0.0	0.0	0.0	70:<80	0.0	0.0	0.0	0.0	
0.0	0.0	0.0	0.0	80:<90	17.6	71.9	18.2	2.0	
5.0	45.5	213.8	52.5	Sum	47.5	193.5	54.5	6.0	
Total trend numbers ($\sum N$)= 11				Total trend lengths ($\sum L$)= 407.3 km					
$\sum N\% = 100\%$				$\sum L\% = 100\%$					

Table 2. Parameters (numbers (N), lengths (L), number and lengths percentages (N% and L%)) of the major fault trends detected from RTP magnetic map

WEST				Azimuth	EAST				
N	N%	L(km)	L%		L%	L(km)	N%	N	
2.0	5.7	30.8	3.8	0:<10	12.3	101.1	11.4	4.0	
2.0	5.7	40.9	5.0	10:<20	4.8	39.2	5.7	2.0	
2.0	5.7	53.3	6.5	20:<30	3.7	30.6	2.9	1.0	
2.0	5.7	60.5	7.4	30:<40	6.6	54.1	5.7	2.0	
1.0	2.9	19.2	2.3	40:<50	3.8	31.1	2.9	1.0	
3.0	8.6	56.6	6.9	50:<60	0.0	0.0	0.0	0.0	
4.0	11.4	100.3	12.2	60:<70	11.1	90.9	8.6	3.0	
0.0	0.0	0.0	0.0	70:<80	4.1	33.3	5.7	2.0	
4.0	11.4	76.8	9.4	80:<90	0.0	0.0	0.0	0.0	
20.0	57.1	438.5	53.6	Sum	46.4	380.2	42.9	15.0	
Total trend numbers (ΣN)= 35				Total trend lengths (ΣL)= 818.7 km					
$\Sigma N\% = 100\%$				$\Sigma L\% = 100\%$					

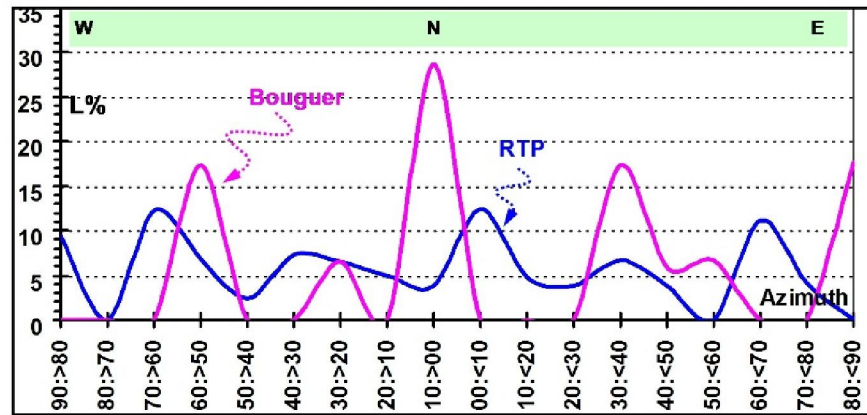


Fig 4. Frequency distribution curves of the gravity and magnetic tectonic trends

3.2.2 Isolation of gravity and magnetic anomalies

To implement the crustal modeling, it is better to remove the effect of shallow-seated causative bodies producing anomalies from the regional ones. The regional- residual separation is applied also to construct the tectonic structure map. Gravity data have been used to study many types of geological structure, ranging in depth and size from very deep crustal blocks to near-surface ore bodies. In general, large regional variations in the Bouguer gravity are related to changes in the thickness of the earth's crust (Woollard 1959 and Osminskaya et al. 1969). In this study, the isolation of gravity and magnetic anomalies into their residual and regional components was carried out using the Fast Fourier Transform (FFT) and least-squares polynomial techniques. These two techniques are used to determine the main structures that are represent in both gravity and magnetic data and cannot determine by using one technique.

Regional- Residual separation using the Fast Fourier Transform (FFT)

The Fast Fourier Transform (FFT) was applied on the magnetic data for calculating the energy spectrum curves and estimating the residual (shallow) and regional (deep) sources. This filter is based on the cut-off frequencies that pass or reject certain frequency values and pass or reject a definite frequency band. Radially averaged power spectrum method is used to determine the depths of volcanic intrusions, depths of the basement complex and the subsurface geological structures. Several authors, such as Lee (1960) and Bhattacharyya (1966) explained the spectral analysis technique.

Results of gravity data

Fast Fourier Transform (FFT) technique is applied to calculate the two dimensional power spectrums and carry out further filtration operations. The power spectrum curves (Fig 5a) show two linear segments related to regional and residual components that are drawn respectively with a blue and red line. Moreover, the inspection of the resulted radially averaged log power spectrum shows low frequency (components < 0.027 cycle/km) reflecting the deep-

seated bodies. The average depth of the regional components tops is about 16km (lower part Fig 5a). High frequency signals (> 0.027 cycle/km) which represent the near-surface contribution (average depth of their tops is about 3km).

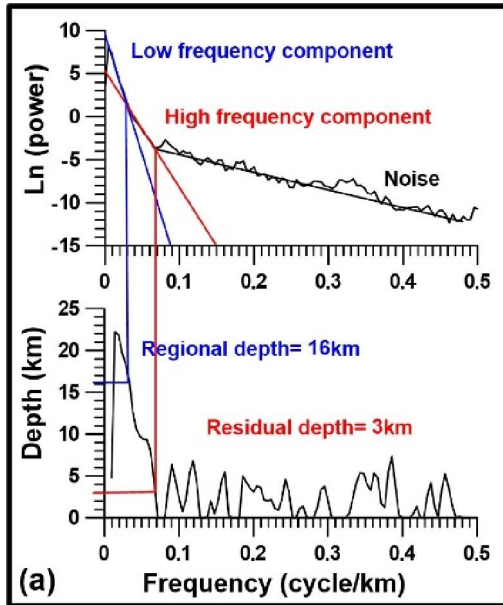


Fig 5a Energy spectra of the gravity data

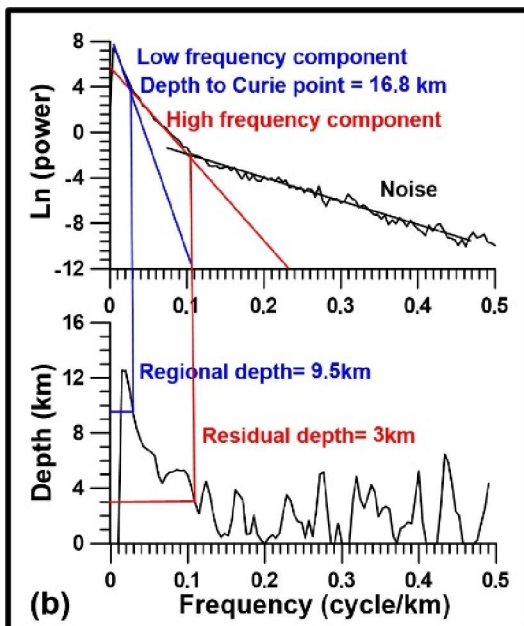


Fig 5b Energy spectra of the RTP magnetic data

The gravity data was filtered to produce the regional and residual component maps (Figs 6 and 7). Figure 6 depicts the deep-seated causative bodies that produce long wavelength gravity anomalies, large areal extent, and high amplitude -45 and 5 mGal. This map shows a large negative gravity anomaly (Fig 6, f)

in the southern part of the study area, trending in N-S direction and amplitude of -45 mGal. Two negative anomalies (d and e) trending in the WNW and ENE directions. On the other hand, this map exhibits two large positive gravity anomalies (b and c) in the middle part; taking ENE direction with amplitude of 5 mGal and WNW direction and amplitude of -6 mGal. In the northern portion of the area, the positive anomaly (Fig 2, a) disappeared completely from the low-pass filtered map (Fig 6). The regional field shows a general increasing northward, which may be related to the thinning of crustal rocks. While, Figure 7 reflects the shallow-seated causative bodies. These alternating positive (Fig 7, a to j) and negative (Fig 7, k to s) anomalies have amplitudes values range from about -6.5 to 6.5 mGal and trending approximately in E-W, NE to ENE and NW to WNW directions. Most of these anomalies have circular, semicircular and elongated shape, reflecting shallow basement relief and supra-basement bodies as well as, the sedimentary cover attitude.

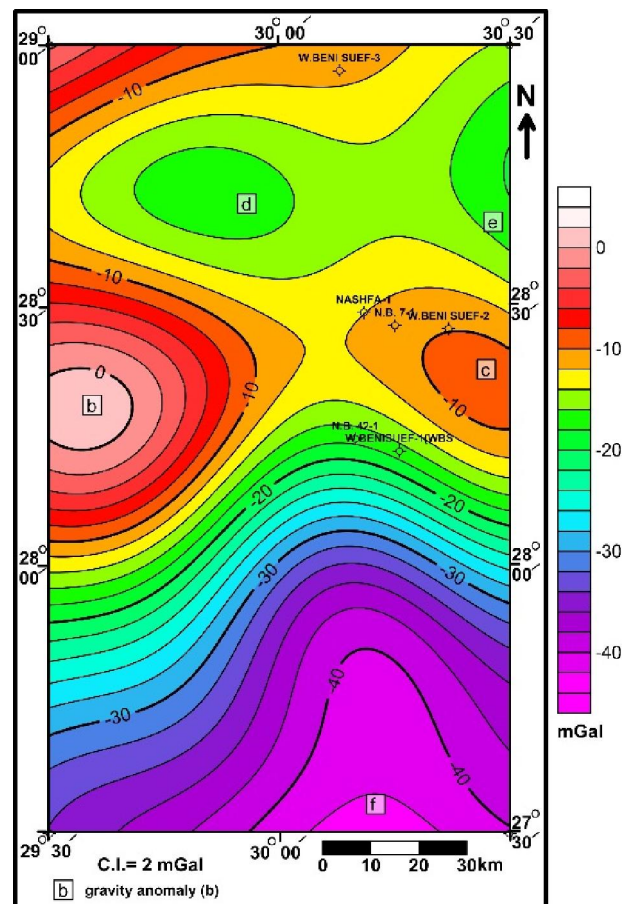


Fig 6 Low frequency gravity map with cutoff 0.027 cycle/km

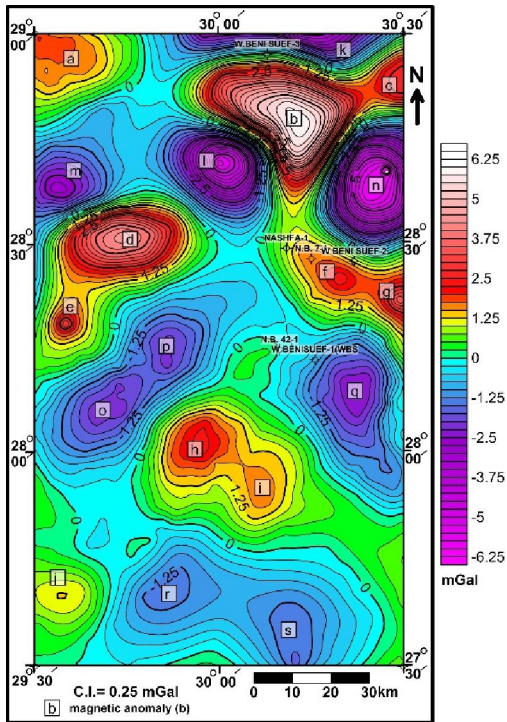


Fig 7 High frequency gravity map with cutoff 0.027 cycle/km

Results of magnetic data:

The power spectrum curve (Fig5b) shows two linear segments related to regional and residual components (respectively with a blue and red line). Moreover, the inspection of the resulted radially averaged log power spectrum shows that: firstly a regional components (lower frequency) less than 0.030 cycle/km reflect the deep seated bodies (about 9.5 km depth). Moreover, the higher frequencies lie more than that frequency, which represent the near-surface contributions with average depth to their tops of about 3km. These maps are shown in Figs 8 and 9.

3.2.3 Least-squares polynomial technique:

The least-squares polynomial fitting is used to separate the Bouguer gravity and RTP magnetic maps into regional and residual components. The resulting maps are very useful in choosing the particular anomalies to be analyzed and in proving some control on the choice of the regional component, as indicated by the low order of surface fitting (Nettleton 1976). Five orders of the fitting polynomial are carried out on the potential field. The correlation factors between successive least-squares residual (or regional) gravity and magnetic anomalies are useful tools maybe is better for detecting the best separation surface defining regional and residual components of the potential data (Abdel-Rahman et al. 1985).

Application of Least-squares polynomial technique on gravity data

The residual map of this order (Fig 10) illustrates a good separation of the residual component, where the positive (a, b and c) and negative (d to h) closed anomalies are well represented. Correlation coefficients results show that, this map is the optimum one (Abdel-Rahman et al. 1985), $r_{23} = 0.957$ (Table 3).

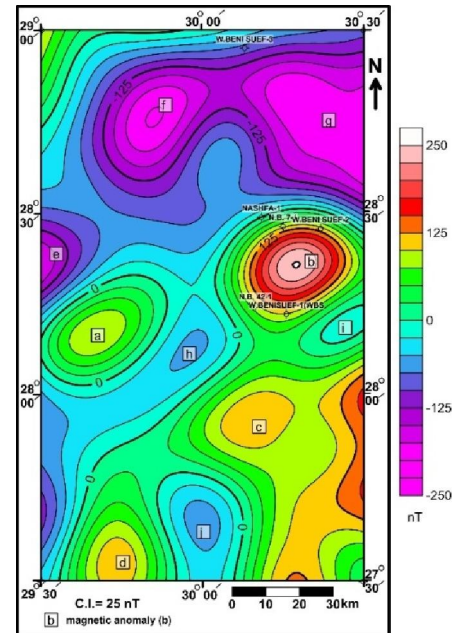


Fig 8 Low frequency magnetic map with cutoff 0.030 cycle/km

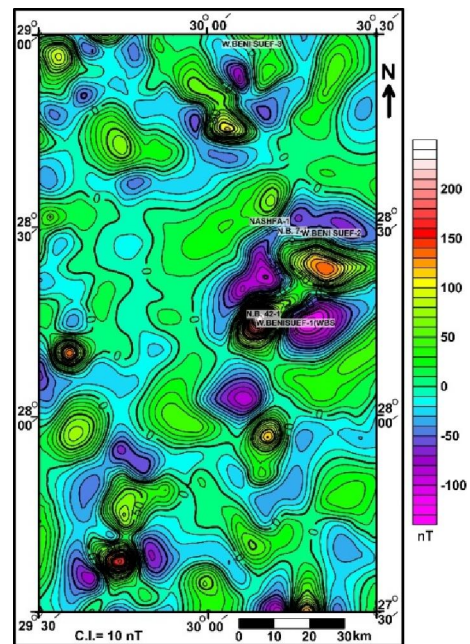


Fig 9 High frequency magnetic map with cutoff 0.030 cycle/km

Table 3. Correlation coefficients of residual gravity maps using the least-squares polynomial technique

	1 st order	2 nd order	3 rd order	4 th order	5 th order
1 st order	1				
2 nd order	0.716	1			
3 rd order	0.687	0.957	1		
4 th order	0.400	0.605	0.630	1	
5 th order	0.396	0.601	0.629	0.899	1

Application of Least-squares polynomial technique on magnetic data

Figure (11) shows the optimum residual surface of the least-squares polynomial technique (Table 4). Generally, residual map shows alternated positive and negative anomalies running mainly in ENE and NE with E-W and NW trends in parts. The map reflects the short wavelengths anomalies that represent the local structures.

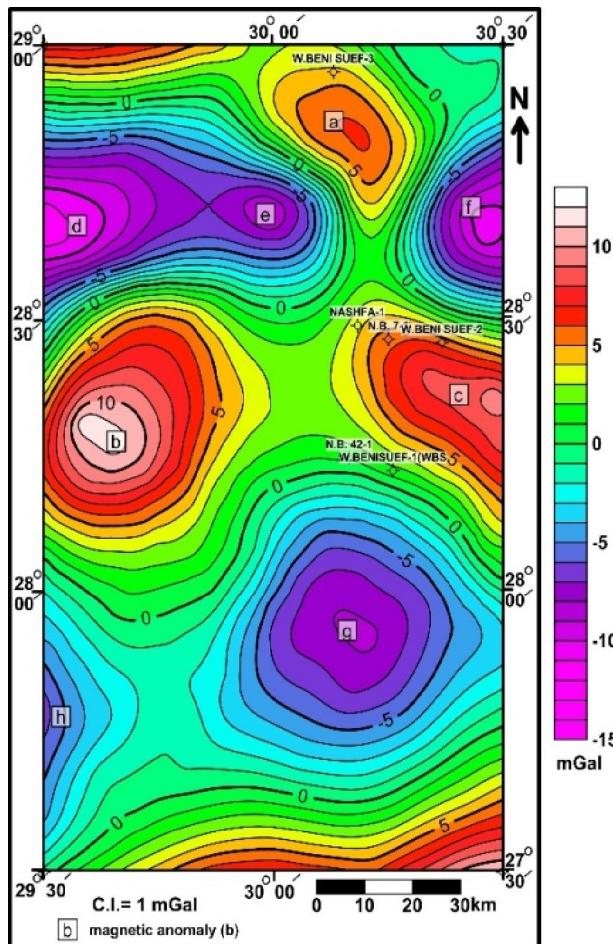


Fig 10. Residual of Bouguer anomaly map with the second order polynomial

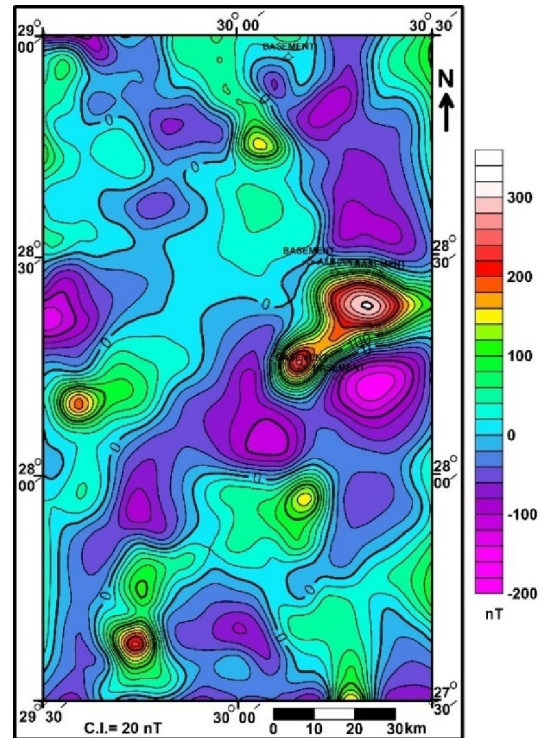


Fig 11. RTP magnetic map with the fourth order polynomial residual surface

Table 4. Correlation coefficients of residual magnetic maps using the least-squares polynomial technique

	1 st order	2 nd order	3 rd order	4 th order	5 th order
1 st order	1				
2 nd order	0.921	1			
3 rd order	0.844	0.916	1		
4 th order	0.713	0.776	0.846	1	
5 th order	0.727	0.793	0.866	0.960	1

3.2.4 Basement Structures Map

The residual maps are used to construct the basement structural map (Fig 12), where the residual positive anomaly can be interpreted as uplifted block while the negative one can be interpreted as down-faulted block. It shows two sets of faults affecting the study area. The first sets are normal faults trending in the NE- SW directions forming alternating uplifted and down-faulted blocks intersected with the younger three transform faults (TF₁, TF₂ and TF₃) taking the NW-SE to NNW-SSE directions. Generally, the area contains many horsts or uplifted blocks belts labeled H₁ to H₅, as well as grabbens or down-faulted block belts labeled L₁ to L₅, as shown in Figure (12). The uplifted block H₃ can be considering as the main uplift located at the middle part of the area.

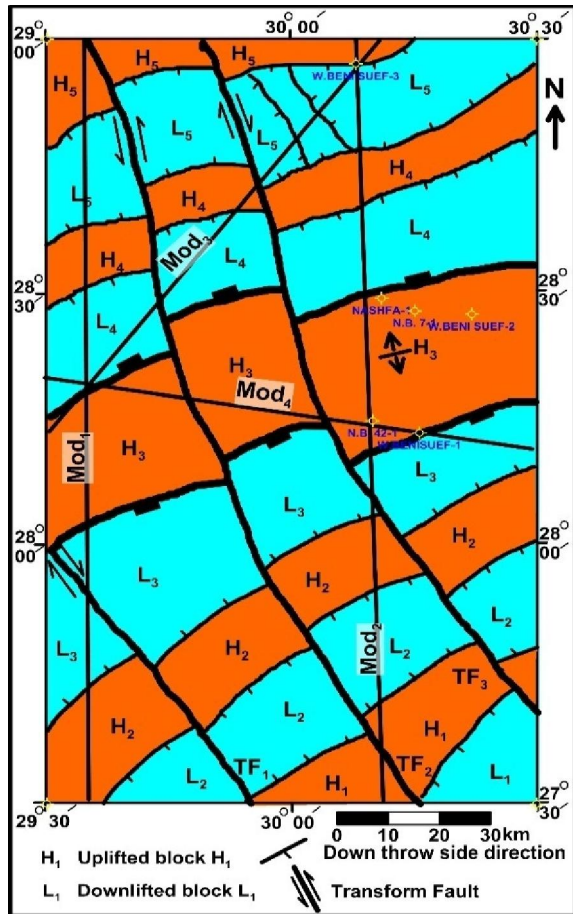


Fig 12. Interpreted structural basement map

3.2.5 Depth Estimation Methods

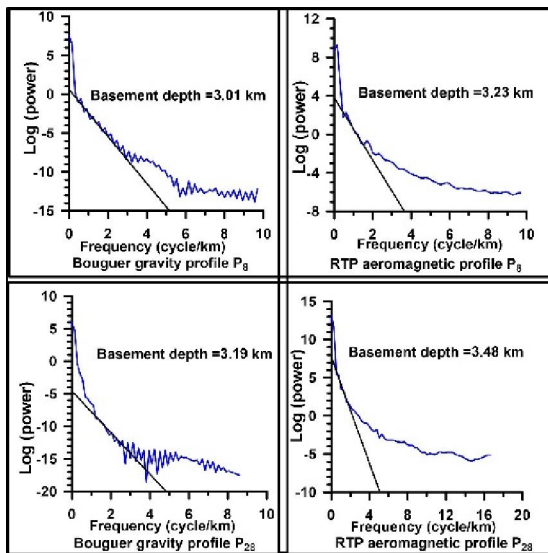


Fig 13. Spectral analysis along profiles P₈ and P₂₈ as examples using Spector and Grant (1970) technique

The results of depth estimation can give information concerning the thickness of the sedimentary succession. Consequently, it is possible to delineate the configuration of the sedimentary basins in the study area. Twenty-eight profiles for both gravity and magnetic maps covering almost the study area are used to estimate the depths to the basement surface using the spectral analysis technique (Spector and Grant 1970). The locations of these profiles are shown in Figure (2). Figure (13) illustrates two examples for the spectral analysis calculation along two gravity profiles (P₈ and P₂₈) and the same location of these profiles on magnetic map. All the results of spectral analysis technique are tabulated in Table (5). This table shows that, the basement depths range from 1.21 km (P₂) to about 3.35 km (P₁₉). The minimum and the maximum values as well as the arithmetic mean and the standard deviation are shown in Table (5) for gravity, magnetic and average values.

Table 5. Results of depth estimation using spectral analysis technique

Profiles name	Basement depth (km) Gravity	Basement depth (km) RTP	Average Basement depth (km)
P ₁	2.58	2.7	2.64
P ₂	1.44	0.98	1.21
P ₃	1.42	1.21	1.315
P ₄	2.39	1.6	1.995
P ₅	1.98	1.92	1.95
P ₆	2.07	1.52	1.795
P ₇	2.1	2.58	2.34
P ₈	3.01	3.23	3.12
P ₉	3.01	2.64	2.825
P ₁₀	3.04	2.86	2.95
P ₁₁	3.01	3.45	3.23
P ₁₂	2.74	2.29	2.515
P ₁₃	3.34	3.1	3.22
P ₁₄	3.22	3.09	3.155
P ₁₅	2.27	1.34	1.805
P ₁₆	2.86	2.22	2.54
P ₁₇	1.75	1.28	1.515
P ₁₈	2.7	2.38	2.54
P ₁₉	3.02	3.68	3.35
P ₂₀	1.86	1.74	1.8
P ₂₁	2.33	2.66	2.495
P ₂₂	2.57	2.23	2.4
P ₂₃	2.59	2.46	2.525
P ₂₄	3.12	2.56	2.84
P ₂₅	2.29	1.32	1.805
P ₂₆	1.81	1.97	1.89
P ₂₇	2.03	1.81	1.92
P ₂₈	3.19	3.48	3.335
Minimum			
Maximum	1.42	0.98	1.21
Mean	3.34	3.68	3.35
Standard deviation	2.491	2.296	2.394
	0.557	0.756	0.63

3.2.6 The gravity and magnetic modeling

Gravity data depend on crustal structure, crustal density (composition) and surface elevation. For regional scale, Bouguer anomalies may be sufficiently clear to give evidence of changes in mass discontinuities in the crust and upper-mantle, as well as the distribution of isostatic balance (Tealeb and Riad 1986). Recent studies indicate that, the Bouguer anomalies and surface relief are closely connected in general with the crustal thickness (Woollard 1959; Pick et al. 1973; Riad et al. 1983 and Riad & El-Etr 1985). However, gravity data alone cannot yield unique solution for density distribution in the earth's interior (Tealeb and Riad 1986).

Magnetic data are due to the Mineralogical composition of the underlying rocks. The depth of magnetized rocks is controlled by the Curie

temperature at which the rock losses its polarization. Figure (5b) indicates that the depth to the source bottom is recorded where a maximum peak is represented (Hinze et al., 2013). The maximum slope of this figure is divided by (4π) to estimate the depth to Curie point isotherm (about 16.8 km). Morgan et al. (1977) study the geothermal gradient in north Egypt and the Gulf of Suez using the drilled oil wells. According to these data, the depth to Curie temperature in the study area ranges from about 16.8 to 18 km.

The densities of the crustal models of the study area were defined through the comparison and correlation of rock density values used in several studies (Table 6) that carried out on the northern part of Egyptian Western Desert, Nile delta and Mediterranean Sea.

Table 6. Correlation of rock density (g/cc) values used in several studies

Layer	Jacobs et al. 1959	Makris 1976	Ginzburg, and Ben Avraham 1987	Abdel-rahman et al. 1988	Setto 1991	Makris et al. 1994	Omran and Fathy 1998	Ismail 1998	Omran 2000	El-Khadragy et al. 2010	Salem et al. (2004); Saada et al. (2014)
Sediments	-----	-----	2.50	2.45	2.46	2.36	2.30	2.40	2.37	2.42-2.44	U 2.10 L 2.50
Intrusions	-----	-----	-----	-----	-----	-----	-----	-----	-----	2.62-3.14	-----
U. Crust	2.67	2.82	2.80	2.68	2.68	2.82	2.67	2.70	2.67	2.73-2.75	2.7
L. Crust	3.00	2.90	2.96	2.90	2.90	2.90	3.00	3.10	3.07	2.91-2.94	2.93
U. Mantle	3.30	3.34	3.25	-----	3.30	3.38	3.30	3.47	3.44	3.23-3.33	3.33

Results of the coupled gravity and magnetic modeling

In the present study, the same density values (Table 6), which mostly based on deep seismic refraction and well logging data, are used as an average values to constrain the 2-D gravity models. Sediments are divided into upper (Miocene to Recent) and lower (pre-Miocene) parts with densities of 2.1 and 2.5 g/cc, respectively (Salem et al. 2004) as an average of sediments. According to (Table 6), the densities of 2.71, 2.93, and 3.33 g/cc are used for lower part of upper crust, lower crust, and upper Mantle, respectively. Moreover, the upper crust is divided into two portions, the upper one is magnetized ranges in depth from 16.8-18.1 km to the basement surface with different magnetic susceptibilities and densities for each rock block, while the lower portion has no magnetic susceptibility (above Curie temperature) and density of 2.71gr/cc.

The well-known depths of basement wells (Fig 1 and Table 7) that were used as starting points confine the modeled profiles. In addition, the constructed structure blocks (Fig 12) as well as the estimated depth to Curie point (Fig 5b) also confines the extension and the geometry of the modeled blocks.

Table 7. The drilling well data

Well	Base TD of well	Total Depth (km)
W. Beni Suef-3	Basement	1.3
N. B. 42-1	Basement	2.16
Nashfa-1	Basement	0.73
N.B. 7-1	Albian	1.07
W. Beni Suef-1	Basement	2.07
W. Beni Suef -2	Basement	2.09

The first modeled profile (Mod₁) trends S-N direction and crosses profiles Mod₃ and Mod₄. It passes through the strongest gravity anomaly in the middle part of the study area (+4 mGal) and decreases to the south (-33 mGal) while, magnetic profile values range from about -130nT to 208nT from south. This profile has been modeled using seven blocks (Fig 14), with density values ranging from 2.64 g/cc (H₄) to 2.77 g/cc (H₅). On other hand, magnetic susceptibility ranges from 0.001 cgs unit (H₂ and H₄) to 0.004 cgs unit (H₃). To display the upper and lower sediments as well as the basement surfaces configurations, the depth ranges from 0 to 8km is magnified below each crustal-modeled profile as shown in (Figs 14-17). The minimum depth to the basement surface is 0.7 km in the southern part, while the maximum depth is 4.12

km at the central part (H_3) and the moderate depth is 2 Km at the northern part (H_4 , L_4 and H_5). The proposed blocks indicate that, the basement surface and the overlying sedimentary cover are affected by normal

faults with different throws and dip angles. The depth to Conrad and Moho discontinuities decreases from 24 km to 21.5 km and from 30.5 km to 33 km, respectively to the north.

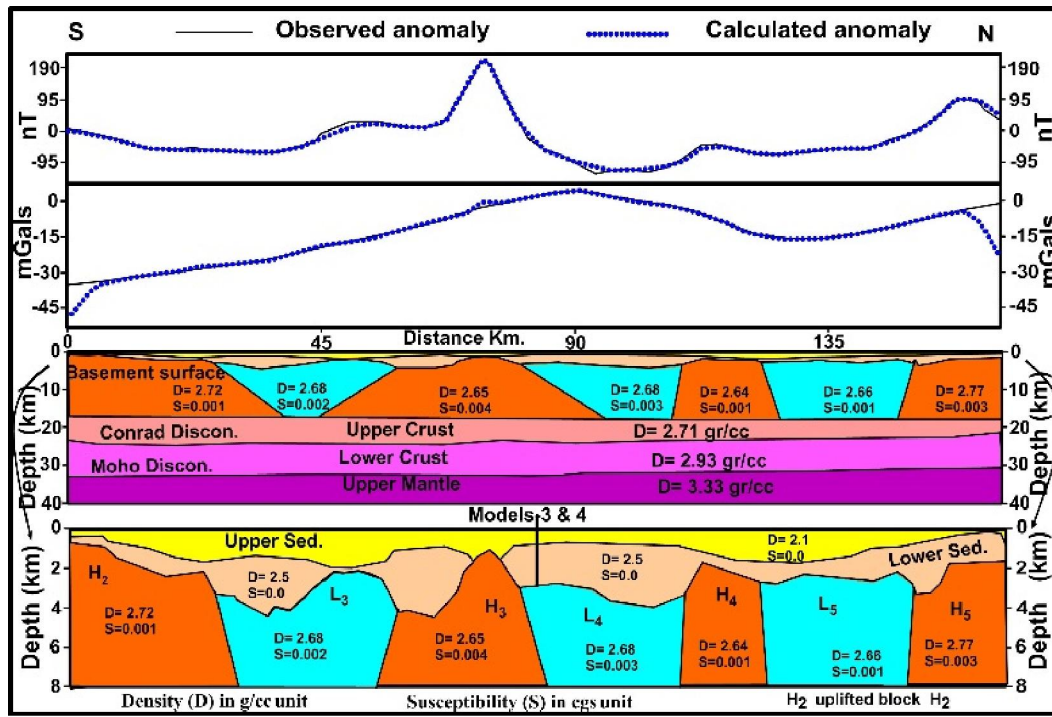


Fig 14. Crustal model along profile Mod₁

The second modeled profile (Mod₂) trends in the S-N direction and crosses profiles Mod₄ at W. Beni Suef-1 well and Mod₃ at W. Beni Suef -3 well. It passes west to Nashfa-1 well at 4km distance. The data of the drilled wells (Fig 1) in the study area that used in modelling process are shown in Table (7). This profile runs through the minimum gravity anomaly in southern part of the study area (-44 mGal) and increases to the north (+7 mGal) while, magnetic profiles values range from about -175 nT at the north to 300 nT at the middle part. The observed and the calculated fields show a good fitting except for the southern part of calculated gravity field due to the edge effects. This profile has been modeled using nine uplifted and down faulted blocks (Fig 15), with density values ranging from 2.65 g/cc (H_2) to 2.77 g/cc (H_1 , L_5 and H_5), while magnetic susceptibility ranges from 0.003 cgs unit (L_5) to 0.01 cgs unit (H_2 and H_3). The minimum depth to the basement surface is 0.5 km at

H_5 , while the maximum depth is 3.9 km at the H_3 . The crustal thickness (depth to Moho discontinuity) varies from 31 km in the southern part to about 34 km in the northern part.

The third modeled profile (Mod₃) is running in the SW-NE direction and passes through W. Beni Suef-3 well. This profile has been modeled using seven blocks (Fig 16), with density values ranging from 2.66 g/cc (H_3 and H_4) to 2.77 g/cc (H_5), while magnetic susceptibility ranges from 0.01 cgs unit (L_5) to 0.01 cgs unit (H_3). The minimum depth to the basement surface is 0.65 km at the uplifted block H_5 (Fig 12) to the north, while the maximum depth is 4.7 km at the down-faulted block L_4 . This crustal model shows a small thickness variation of crustal rocks. The depth to Moho discontinuity ranges from 31.5 km to 33km in the southwestern part. In addition, the depth to Conrad decreases from 24 km to 22 km in the northeastern portion.

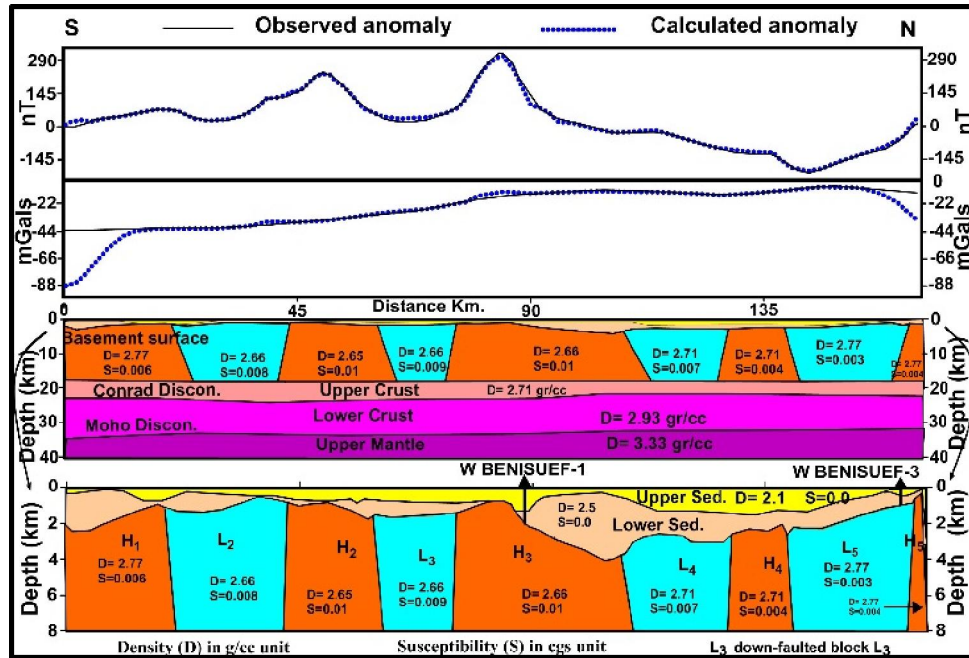


Fig 15 Crustal model along profile Mod₂

The fourth modeled profile (Mod₄) is running in the WNW-ESE direction and passes through N.B. 42-1 and W. Beni Suef-1 wells, in the middle part of the study area. It has been modeled using four blocks (Fig 17), with density values ranging from 2.66 g/cc (L₃) in eastern portion to 2.68 g/cc (L₄) in the western part, while magnetic susceptibility ranges from 0.003 cgs unit (L₄) to 0.01 cgs unit (H₃). The dashed line of the

main uplifted block H₃ illustrates a lateral change in density values from 2.68 to 2.66 g/cc eastward. The minimum depth to the basement surface is 1.2 km at the down-faulted block L₃ to the ESE direction, while the maximum depth is 4.5 km at the uplifted block H₃. The maximum depth of Moho is presented in the middle part.

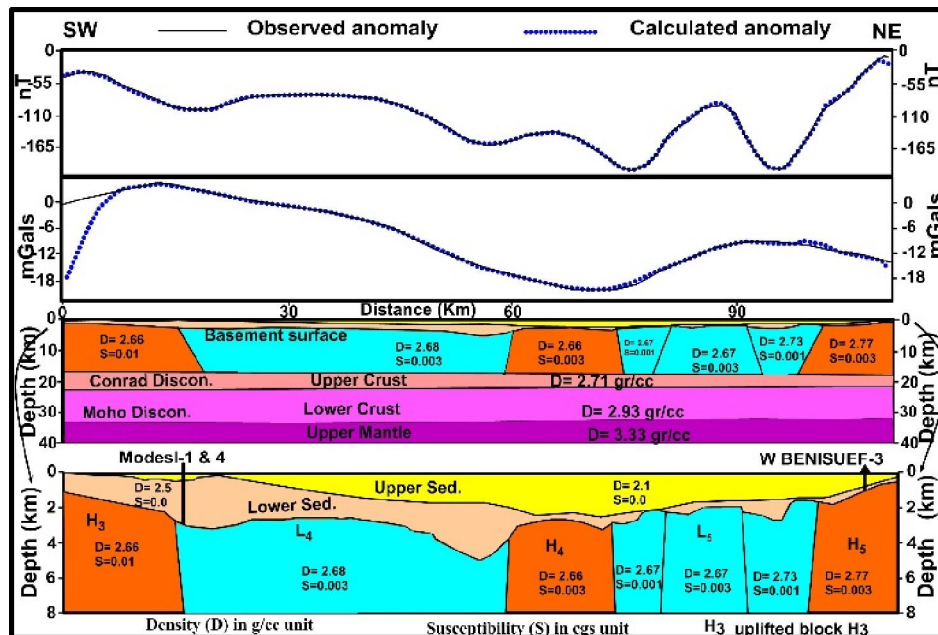


Fig 16 Crustal model along profile Mod₃

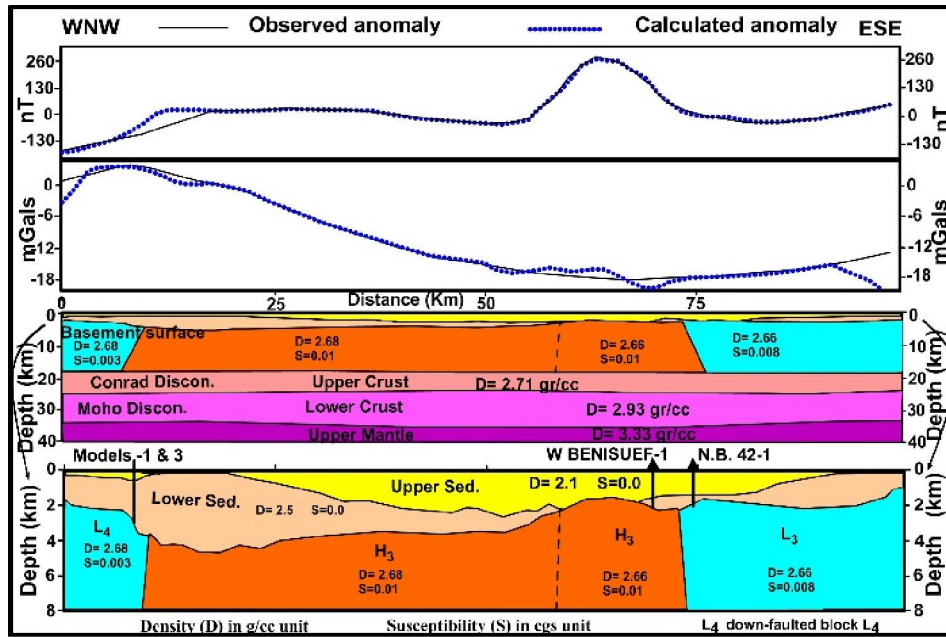


Fig 17 Crustal model along Profiles Mod₄.

The modeled profiles (Figs 14 to 16) show a general decreasing for the thickness of the crust to the north direction. Woodside and Bowin (1970) reported a gravity profile along Longitude 31°E, postulating that the depth of Moho is about 23 km at the Egyptian coast in the south of the Mediterranean Sea. Therefore, the decreasing of Moho depth is acceptable northward.

3.2.7 The Basement relief map:

This map is to focus the depths change of the basement surface. It is constructed depending on the available wells reached to the basement and the data derived from all the depths estimated using the spectral analysis technique, as well as the data digitized from four gravity and magnetic models.

In this map, five drilled wells reached to the basement surface as shown in Figure (1) and Table (7), and the calculated depths to the basement deduced from 28 gravity and magnetic (P₁ to P₂₈) profiles, as shown in Table (5), are used to construct this map. The locations of these profiles are illustrated in Figure (2). In addition, the depths to the basement surface are digitized from four gravity and magnetic models (Mod₁ to Mod₄) to construct the basement structure relief map (Fig 18). It shows shallow depths in the southeastern and the northern parts. The minimum depths in the area lie in the extreme north (uplifted block H₅), north to W. Beni Suef-3 well (about 0.6km), and around Nashfa-1 well (0.73km) in the eastern part of the uplifted block H₃ as well as eastern portion of the down-faulted block L₃. On the other hand, maximum depths (4.2km) are presented in the western portions of the middle part (in the down-

faulted blocks L₃ and L₄), indicating a thick sedimentary basin trending in the NE direction.

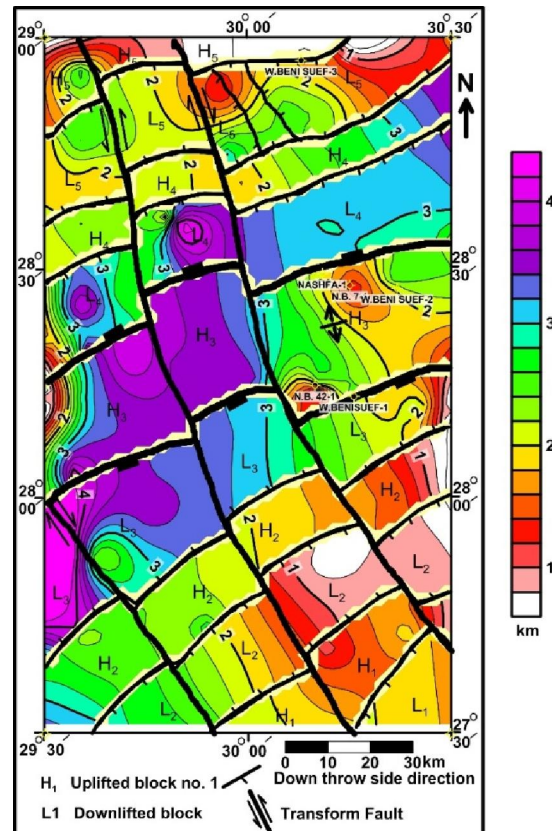


Fig 18. Structural basement relief map

Finally, both gravity and magnetic results are accordance with each other. The application of different analytical techniques on the potential field data helps us to understand the geologic evolution of the study area. Where, trend analysis technique determined the main trends that intersected the study area. The regional-residual separation methods are used to reveal the uplifted and the down-faulted blocks as well as the transform faults of the investigated region. The coupled 2D/2.5D-gravity and magnetic modeling is carried out to study the crustal thickness variation and to delineate the densities and the magnetic susceptibilities of the revealed uplifted and down-faulted blocks. In addition, a structural basement relief map is constructed using the depths of the available basement drilled wells, spectral analysis profiles and modeled profiles.

4. Summary and Conclusions

The application of the different analytical technique on both gravity and magnetic data, leads to conclude that:

1) The area is affected by the following trends ENE (Syrian Arc), E-W (Tethyan), WNW (Najd) and N-S (East African).

2) The regional – residual separation technique is carried out on the Bouguer gravity and the RTP magnetic maps, in order to separate shallow anomalies (structures) from the deeper ones. FFT and least-squares polynomial techniques are applied to achieve this goal. Low and high frequencies gravity maps less and more than 0.037 cycle/km are constructed respectively to delineate the regional and residual components. Magnetic maps are constructed below and above 0.030 cycle/km. Both of them show alternative positive and negative closed anomalies all over the area. The least-squares polynomial technique results are correlated at the different levels (1st to 5th) by calculating the correlation coefficients. These coefficients indicate that, the regional-residual separation map at the second order is the optimum one of gravity data and the fourth are the best one for magnetic data. The residual maps of the least-squares polynomial technique are useful for constructing the basement structure map, where regional components were removed.

3) The structural map is constructed, using the results obtained from the regional- residual separation techniques of both gravity and magnetic data. According to this map, the area is formed from alternative uplifted and down-faulted blocks trending in the ENE direction. A younger NNW to NW transform faults (can be related to the Gulf of Suez) intersects these old uplifted and down-faulted blocks.

4) The depths to the basement rocks are calculated along the same 28 gravity and magnetic profiles covering the study area, using the spectral

analysis technique. The depth to basement varies from one place to another. It ranges from 1.2 to 3.4 km.

5) Four models (2D and 2.5D gravity and magnetic) are constructed to show the subsurface imaging and geometry of the upper and lower sediments, magnetic layer, upper and lower crust as well as upper mantle. The density values of 2.1 g/cc and 2.5g/cc are used for the upper and lower sedimentary layers. While the densities of 2.71, 2.93, and 3.33 g/cc are used for the upper crustal layer (beneath the magnetic layer), the lower crustal layer (basaltic layer) and the upper mantle layer, respectively. The magnetic layer (from basement surface to Curie temperature depth) is divided into the uplifted and the down-faulted blocks with different densities (from 2.64 to 2.77 g/cc) and magnetic susceptibilities (from 0.001 to 0.01 cgs unit).

6) These models show that, the thickness of the upper sediments ranges from 0.0 to 2.45 km, while the depth to basement surface ranges from 0.5 to 4.2 km. They show also that, the depth to Curie temperature vary from 16.8 to 18.1km, depth to Conrad discontinuity ranges from 21.2 to 24.7km, while the depth to Moho discontinuity varies from 30.5 to 34.9km. The thickness of the crust shows a general decreasing northward, in agreement with different modeled profile carried out by many authors (e.g. Salem et al. (2004), Saada et al. 2014 and others).

7) An integrated basement structural relief map is constructed using the average depths estimated from the spectral analysis technique (28 profiles) and five basement wells, as well as to four gravity and magnetic models. It shows a minimum basement depth in the northern part with a depth of 0.6 km (the northern uplift) and in the eastern uplifted portion of the area. While the western down-faulted blocks of the middle part have, the maximum depths attain of about 4.2 km.

References

1. Abdel Aal AA, Moustafa, AR (1988). Structural framework in Abu El Gharadig Basin, Western Desert, Egypt. EGPC, 9th Expl Conf Cairo, Egypt.
2. Abdel Gawad M (1970) The Gulf of Suez, a brief review of stratigraphy and structure. Phil Trans Roy Soc Lond A 267: 23-40.
3. Abdel- Rahman SM, Riad S, Refai EM, Amin Y (1985) On the leastsquares residual anomaly determination. Geophysics 50: 473-480.
4. Abdelrahman EM, Refai EM, El-Ghalban HM (1988) Gravity models of the Nile Delta basin, Egypt. EGS proc of 6th Ann Meet 27-42.
5. Abu El-Ata ASA (1981) A study on the tectonics and oil potentialities of some Cretaceous- Jursic basins, Western Desert, Egypt; using geophysical

- and subsurface geological data. Ph. D. Thesis Fac Sci Ain Shams Univ.
6. Abu El-Ata ASA (1988) The relation between the local tectonics of Egypt and plate tectonics of the surrounding regions, using geophysical and geological data. EGS Proc of 4th Ann Meet 103-123.
 7. Affleck L (1963) Magnetic anomaly trend and spacing patterns. *Geophys* 28: 379 - 395.
 8. Barakat MG (1984) General review of the petroliferous provinces of Egypt with special emphasis on their geologic setting and oil potentialities. Petrol and Gas Proj Cairo Univ MIT Technology planning program.
 9. Bhattacharyya BK (1966) Continuous spectrum of the total-magnetic field anomaly due to a rectangular prismatic body. *Geophysics* 31: 97-121.
 10. Dennis SW (1984) The tectonic framework of petroleum occurrence in the Western Desert of Egypt. EGPC 7th exploration seminar Cairo.
 11. Dietz RS and Hoden JC (1970) Reconstruction of Pangea, break-up and dispersion of continents, Permian to present. *J Geophys Res* 75: 4939-4955.
 12. Dolson JC, Shann MV, Matbouly S, Harwood C, Rashed R, and Hammouda H (2001) The Petroleum Potential of Egypt. In WA Morgan (editor), *Petroleum Provinces of the 21st Century*, Memoir V, 74. Tulsa, Oklahoma, American Association of Petroleum Geologists 453-482.
 13. Egyptian Geological Survey and Mining Authority (1981) Geologic map of Egypt, scale 1:250,000.
 14. El-Kenawy AA (2000) Interpretation of potential field data of the area between latitudes 27° 30' - 29° 00'N and longitudes 26° 00'E, Western Desert, Egypt. Ph. D. Thesis Fac Sci Zagazig Univ.
 15. El-Khadragy A A, Saad M H, Azab A (2010) Crustal Modeling of South Sitra Area, North Western Desert, Egypt Using Bouguer Gravity Data. *J App Sci Res* 6: 22-37.
 16. El-Shazly EM, Abdel Hady MA, Salman AB, Morsy MA, El-Rakaiby MM, El-Ansary IA, Meshref WM, Ammar AA, Meleik ML (1975) Geological and geophysical investigations of the Suez Canal zone. ASRT, Remote sensing center, Cairo, Egypt.
 17. General Petroleum Company (1984) Gravity map of Egypt with of scale 1:250,000. Egyptian Academy of Scientific Research and Technology, Cairo.
 18. General Petroleum Company (1989) Magnetic map of Egypt with of scale 1:250,000. Egyptian Academy of Scientific Research and Technology, Cairo.
 19. Ginzburg A, Ben Avraham Z (1987) The deep structure of the central and southern Levant continental margin. *Ann Tectonicae* 1: 105-115.
 20. Halsey JH, Gardner WC (1975) Tectonic analysis of Egypt using Earth Satellite data. Lecture given to Egyptian Petrol Geol Cairo GPC.
 21. Hantar G (1990) North Western Desert. In R Said (editor). *The Geology of Egypt*. (Rotterdam, Netherlands, AA Balkema Publishers) 293-319.
 22. Hinze WJ, Von Frese RRB, Saad AH (2013) *Gravity and Magnetic Exploration Principles, Practices, and Applications*. Cambridge Univ Press.
 23. Ismail MA (1998) Geophysical studies in northern part of Egypt. Ph.D. Thesis Cairo University.
 24. Jacobs JA, Russall RD, Tuzo WJ (1959) *Physics and Geology*. McGraw-Hill Tronto.
 25. Lee YW (1960) *Statistical theory of communication*. Willey and Sons, New York, 1 - 75.
 26. Makris J (1976) A dynamic model of the Hellenic Arc deduced from geophysical data. *Tectonophysics* 36: 339-346.
 27. Makris J, Wang S, Odintsov D, Udintsov GB (1994) The magnetic field of the eastern Mediterranean Sea. In Cruise 5 of the research vessel 'Akademik Nikolaj Strakhov' Geolog. Survey of Israel report 87-98.
 28. Meshref WM (1982) Regional structure setting of the Northern Egypt. EGPC, 6th Exploration Seminar, Cairo, Egypt.
 29. Meshref WM (1990) Tectonic framework of Egypt. In R Said (editor). *The geology of Egypt* (Rotterdam, Netherlands, Balkema A A Publishers) 113-130.
 30. Meshref WM (1995) Well evaluation conference of Egypt. Schlumberger Technical Editing Services, EGPC, Egypt.
 31. Meshref WM (2002) Basement tectonic map of Egypt. Cairo 2002 international petroleum conference and inhabitation, Cairo 1-5.
 32. Moody GB (1961) *Petroleum exploration Hand book*, Mc-Graw-Hill Book Co Inc New York.
 33. Morgan P, Blackwell DP, Farris JC, Boulos FK, Salib PG (1977) Preliminary geothermal gradient and heat flow values for north Egypt and Gulf of Suez from oil well data. Proc Intl Congr Thermal Waters, Geothermal Energy and Volcanism of the Mediterranean area (1976), Nat Tech Athens, 424-438.

34. Nettleton LL (1976) Gravity and magnetic in oil prospecting. Mc-Graw-Hill Book Co. Inc., New York.
35. Omran MA, Fathy H (1998) Structural evolution of the Nile cone area. *Egypt J Geology* 42: 273-291.
36. Omran MA (2000) Crustal modeling of the continental margin of the Nile Delta region. *Ann Geol Surv of Egypt* 23: 381-387.
37. Osminskaya IP, Belyaevsky NA, Volvovsky IS (1969) Explosion seismology in the USSR; in P J Hart (editor), *The Earth's Crust and Upper Mantle*. Geophysical Monograph 13: 195-208, American Geophysical Union, Washington, DC.
38. Pick M, Picha J, Vyskocil V (1973) Theory of Earth's gravity field. Academia, Publ House of Czechoslovak academy of sciences.
39. Riad S, El-Etr HA (1985) Bouguer anomalies and lithosphere- crustal thickness in Uganda. *Journal of Geodynamics* 3: 169-186.
40. Riad S, Fouad A, Refai E, Ghaleb M (1983): Preliminary interpretation of regional gravity anomalies of Egypt. Paper presented at the 8th General Assembly of the IUGG, Hamburg.
41. Saada SA, Zahra H, El-Khadragy AA (2014) Structural Pattern and Crustal Modeling of the Central Northern Part of Egypt, Using Bouguer Gravity Data. *J App Sci Res* 9, 10: 6373-6386.
42. Said R (1962) *The Geology of Egypt*. Amsterdam.
43. Salem SR, El-Khateeb SO, Mousa MF (2004) Structure and evolution of North African passive margin crust as inferred from 2-D gravity modeling of Nile Delta and its surrounding areas, Egypt, *EGS Journal*, 2, 17-29.
44. Setto IA (1991) A crustal model for Nile Delta, Egypt. *Egypt J Geol* 34: 279-292.
45. Spector A, Grant FS (1970) Statistical models for interpreting aeromagnetic data. *Geophys* 35: 293-302.
46. Sultan N, Abdel Halim M (1988) Tectonic framework of northern Western Desert, Egypt and its effect on hydrocarbon accumulations; 9th EGPC Expl Conf CONOCO.
47. Tealeb A, Riad S (1986) Regional gravity anomalies of western Saudi Arabia and their geological significance. *EGS Proc of 5th Ann Meet March 29-30*: 50- 89.
48. Woodside J, Bowin C (1970) Gravity anomalies and inferred crustal structure in the Eastern Mediterranean Sea. *Bull Geol Soc Am* 81, 4: 1107-1122.
49. Woollard GP (1959) Crustal structure from gravity and seismic measurements. *J of Geoph Res* 64:1521-1544.
50. Youssef MI (1968) Structural pattern of Egypt and its interrelation. *American Assoc Petrol Geol Bull* 52,4: 601-614.

12/20/2015